JOURNAL OF MATERIALS SCIENCE 28 (1993) 6120–6126

# Prediction of indentation-load dependence of fracture strengths from R-curves of toughened ceramics

N. RAMACHANDRAN, D. K. SHETTY
*Department of Materials Science and Engineering, University of Utah, Salt Lake City, Utah 84112, USA*

Rising-crack-growth resistance or R-curves evaluated by direct measurements of crack lengths associated with indentation flaws in a sintered silicon nitride and a sintered and isostatically hot pressed (HIPed) SiC (whisker)-reinforced alumina were used to predict the corresponding indentation-load dependence of fracture strengths. Two empirical R-curve functions, a power law and an exponential function, were fitted to the R-curve data for the analysis. Fracture strengths were calculated by a combined numerical and graphical procedure that determined the point of tangency between crack-driving forces and the R-curves. The results revealed that the exponential function gave a better prediction of the measured log fracture-strength versus log indentation-load relation than the power law. The exponential function also predicted a nearly linear relation between log fracture-strength and log indentation-load, thus indicating that the apparent linearity of this plot is not adequate evidence to assume a power-law R-curve function. This study, therefore, reinforces the case for R-curve evaluations to be based on direct crack-length measurements rather than strength measurements, because the indentation-load dependence of the fracture strength is not sufficiently sensitive to discriminate between potential R-curve functions.

## 1. Introduction

The discovery of such mechanisms as transformation toughening in zirconia ceramics, whisker reinforcement in alumina and self-reinforcement by elongated grains in silicon nitride has led to the development of a new class of toughened ceramics [1]. The increased fracture toughness of these ceramics is usually reflected in a rising crack-growth resistance or R-curve behaviour [2]. The fracture toughness typically increases from a value of less than 5 to 10 MPa $m^{1/2}$, and higher, with increasing crack growth. Accordingly, the focus in the fracture-toughness characterization of these ceramics is on precise measurements of R-curves pertinent to cracks or flaws that control the fracture strengths of these ceramics.

Two approaches have been used in recent years to assess R-curves for surface cracks in ceramics. Marshall [3], Steinbrech and Schmenkel [4] and Yu and Shetty [5] assessed R-curves for MgO-partially-stabilized zirconia (Mg-PSZ), alumina and $CeO_2$-stabilized tetragonal zirconia (Ce-TZP), respectively, by measuring the stable growth of intrinsic surface cracks. This approach is attractive because the assessed R-curves are directly based on actual strength-controlling cracks. However, this approach is not always easy to implement because of the difficulty in locating the cracks before unstable fracture and the need for a loading device that can be mounted on an optical-microscope stage where stable crack growth can be monitored *in situ*.

To avoid the difficulties associated with locating and monitoring the growth of intrinsic surface cracks, artificial surface cracks produced by Vickers microhardness indentation have been employed in R-curve evaluations [6–11]. The procedure usually involves measuring the fracture strengths of ceramics in four-point bending as a function of the Vickers indentation load and then using this load dependence of the strength to infer the R-curve. Often, measured fracture strengths are shown to decrease as a power function of the indentation load, with the magnitude of the exponent being less than 1/3; this is interpreted as evidence for a simple power-law R-curve; that is, the fracture toughness increases as a power function of the crack length. However, there are several drawbacks with such a procedure, and these have been discussed in recent papers [12–15].

Anderson and Braun [14] and Ramachandran and Shetty [15] have recently used a hybrid procedure that employs Vickers indentation to locate starter cracks. This procedure is similar to that originally used by Cook and Lawn [16]. In a previous study by the present authors [15], R-curves were assessed from direct measurements of crack lengths at different stages: initial crack lengths, $c_0$, obtained on indentation; stable growth of the cracks during far-field loading, $c$; and crack lengths at fracture instability, $c^*$. This procedure obtains R-curves without an *a priori* assumption of the crack-length dependence of fracture toughness, and it thus avoids the limitations asso-



0022–2461 

ciated with the indentation-strength method. In addition, it improves the economy of experimentation, because a large body of data can be obtained from multiple indents on each specimen.

The present paper examines the relation between rising crack-growth-resistance curves and the strength/indentation load relation for a self-reinforced silicon nitride and a whisker-reinforced alumina. The primary objective of this study was to see if fracture strengths measured at different indentation loads could be predicted using analytical fits to the R-curves assessed in our previous study [15]. A combined numerical and graphical procedure was employed to calculate fracture strengths from the points of tangency between the crack-driving force curves and the R-curve. The analysis included the variation of a surface-correction factor for the stress intensity of surface cracks as a function of size and shape. A secondary objective was to examine the sensitivity of these predictions to the analytical functions chosen to fit the R-curves.

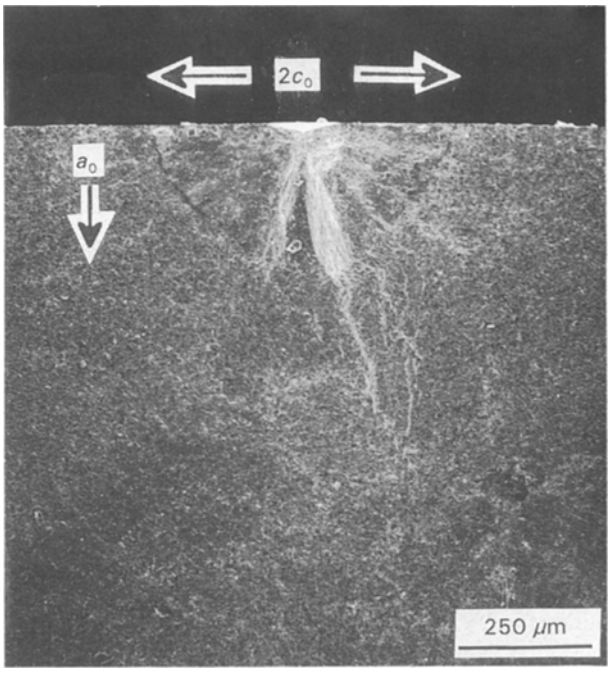


*Figure 1* A surface-crack produced by a Vickers microhardness indentation of SiC(whisker)–reinforced alumina at $P = 298.5$ N.

## 2. Background for analysis

### 2.1. R-curves from stable-crack-growth measurements

The procedures used in measuring R-curves for the two toughened ceramics, a sintered silicon nitride (grade SN-252, Kyocera Industrial Ceramics Corp., 2700 River Road, Des Plaines, IL 60018, USA) and a sintered and HIPed SiC(whisker)-reinforced alumina (experimental grade, Ceramatec Inc., 2425 South, 900 West, Salt Lake City, UT 84119, USA) with 20 vol % whiskers, have been described in detail by Ramachandran and Shetty [15]. The form of the R-curves was essentially defined by the discrete fracture-toughness data obtained from crack-length measurements. A brief summary of the salient features of the analysis is given here.

From the as-indented crack size, $c_0$, measured as a function of the indentation load, $P$, and the subsurface crack depth, $a_0$, measured from the fracture surface of a few selected specimens, the initial cracks were found to be approximately semicircular ($a_0/c_0 \sim 1$). Fig. 1 shows one such half-penny crack in SiC(whisker)-reinforced alumina corresponding to an indentation load of $P = 298.5$ N. Accordingly, the initial surface cracks could be treated as half-penny cracks. The crack-growth resistance based on the initial crack length, $K_R$, was calculated using the following well-known equilibrium relation between the indentation load and the crack size [17]:

$$K_R(c_0) = \delta\left(\frac{E}{H}\right)^{1/2} \frac{P}{c_0^{3/2}} \quad (1)$$

The non-dimensional constant $\delta$ in Equation 1 is dependent on the indenter geometry and the Poisson's ratio of the indented material. Together with the elastic modulus/hardness parameter, $(E/H)^{1/2}$, $\delta$ defines the relation between the applied indentation load, $P$, and the residual crack-opening force of the indentation plastic zone [17]. Based on both theoretical considerations [18] and experimental calibration [15], a value of $\delta = 0.023$ was used in Equation 1 to calculate the crack-growth resistance of both ceramics using the initial crack lengths.

The quasistatic equilibrium during the growth of indentation cracks under the influence of a far-field applied stress, $\sigma$, is described by the following equation [17]:

$$K_R(c) = \delta\left(\frac{E}{H}\right)^{1/2} \frac{P}{c^{3/2}} + 2\Omega\sigma\left(\frac{c}{\pi}\right)^{1/2} \quad (2)$$

It is possible to obtain two more sets of crack-growth-resistance values from Equation 2 by substituting stable crack lengths, $c$, at increasing applied stresses, $\sigma$, as well as the final instability crack length, $c^*$, and the fracture stress, $\sigma_f$. However, the fracture toughnesses calculated from crack lengths measured *in situ* during incremental loading are susceptible to errors. This was evident from the R-curves of our previous study [15] where the fracture toughnesses assessed from incremental crack lengths showed significant scatter. It should be noted that the incremental stresses, $\sigma$, applied during the *in situ* crack-growth measurements were calculated from strain measurements using elastic moduli reported by the material suppliers. Any error in the reported elastic moduli would be carried over as an error in the calculated fracture toughness. Subcritical crack growth during *in situ* measurements can also potentially overestimate the fracture toughness because the measured crack length is not the true equilibrium crack length but is an extended subcritical crack length. Accordingly, the crack-growth-resistance values based on the incremental crack lengths were not included in the present analysis of the R-curves.

In Equation 2, $\Omega$ is a stress-intensity coefficient that accounts for a free-surface correction and stress-gradient effects. $\Omega$ is a function of the crack shape (defined

by $a/c$, where $a$ is the crack depth and $c$ is half the surface-crack length) and the relative crack size (defined by $a/w$, where $w$ is the beam thickness). Experimental evidence [19, 20, 21] and an ASTM standard [22] suggest that surface cracks in beams subjected to bending propagate in such a way that the crack-shape parameter, $a/c$, decreases linearly with the relative depth of the surface cracks:

$$\frac{a}{c} = 1 - \frac{a}{w} \tag{3}$$

Fig. 2 shows a plot of $a/c$ as a function of $a/w$ for surface cracks subjected to pure bending stresses. In Fig. 2, the triangles represent crack-shape data for selected initial indentation cracks from the present study. The circles are data from [20] for fatigue cracks obtained for several types of steels in four-point bending. The squares indicate crack-shape data for cantilever-bending fatigue of an aluminium alloy obtained from [21]. The solid line is a plot of Equation 3. It is clear from Fig. 2 that Equation 3 provides a good correlation with all the experimental data. The crack-shape data measured from the initial indentation cracks in the present study were limited to small values of the relative crack depth, $a/w$. Similar measurements were difficult to make for the cracks close to the instability point $c^*$. However, it is likely that the growth of the initial cracks to their instability sizes under bending stresses would follow the trend for crack-shape change with relative size shown in Fig. 2. Therefore, Equation 3 was used in the present study to define the shape of a surface crack, $a/c$, based on measurements of $c$.

Newman and Raju [21] have reported values of $\Omega$ for different positions along the crack front of a semi-elliptical surface crack of arbitrary shape ($a/c$) and relative size ($a/w$) subjected to bending. Their results, obtained by finite-element analysis and fitted with empirical equations, were employed in the present study to calculate $\Omega$. It should be noted that for semi-elliptical cracks whose shape varies with relative depth, as indicated by Equation 3, $\Omega$ is a maximum at the free surface. These values of $\Omega$ were used

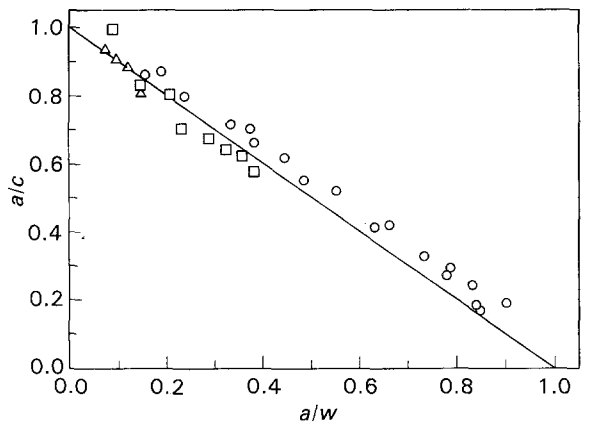


*Figure 2* Variations of the crack-shape parameter, $a/c$ with the relative crack depth, $a/w$ for surface cracks in bending: (△) this study (four point), (○) results from [20] (four point), (□) results from [21] (cantilever), and (—) the graph of $a/c = 1 - a/w$.

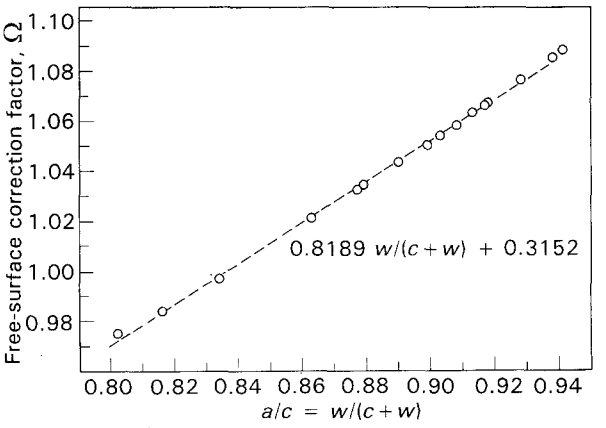


*Figure 3* Variation of the stress-intensity coefficient, $\Omega$, for surface cracks in silicon nitride as a function of the crack-shape parameter, $a/c$, in bending: (○) data obtained by Newman and Raju [21], and (- - -) a linear fit.

in the calculation of the fracture toughness. Because the relation between the shape parameter and the relative crack depth is adequately represented by Equation 3 the stress-intensity coefficient, $\Omega$, calculated using the finite-element results of Newman and Raju [21] could be plotted against a single variable, $a/c$, or equivalently against $w/(c + w)$, measured in experiments. Such a plot for silicon nitride is shown in Fig. 3. In the range of crack lengths measured in experiments, $\Omega$ increased linearly from 0.975 to 1.09 with increasing values of $w/(c + w)$. The discrete points shown in Fig. 3 were used to calculate the crack-growth resistance, $K_R$, in Equation 2, while a linear fit given by the following equation (represented by the dashed straight line in Fig. 3) was used in the strength prediction:

$$\Omega = \frac{0.8189w}{(c + w)} + 0.3152 \tag{4}$$

The $\Omega$-values for SiC(whisker)-reinforced alumina showed a similar linear variation and the following equation was fitted:

$$\Omega = \frac{0.7722w}{(c + w)} + 0.3564 \tag{5}$$

Equations 4 and 5 (both linear) were used to include the variation of $\Omega$ as a function of crack length in the strength analysis of the two ceramics. However, in reality, the variation of $\Omega$ as a function of the normalized variable $w/(c + w)$ is slightly non-linear. Such non-linearity is evident from Fig. 3. Equation 4 is different from Equation 5 because of the difference in the applicable ranges of $a/c$ or $w/(c + w)$, between SiC(whisker)-reinforced alumina and silicon nitride over which the linear fits to the discrete $\Omega$-values were obtained.

## 2.2. R-curves for silicon nitride and SiC (whisker)-reinforced alumina

Figs 4 and 5 show fracture-toughness measurements as functions of crack length, that is, R-curves, assessed from the initial and the instability crack lengths for the

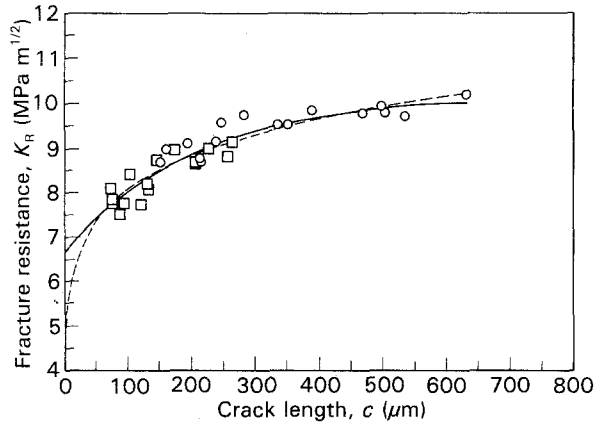


*Figure 4* Rising crack-growth-resistance (R-Curve) for silicon nitride: (⊡) initial crack length, $c_0$; (⊙) instability crack length, $c^*$; (—) exponential fit (crack-length data); and (- - -) power-law fit (crack-length data).

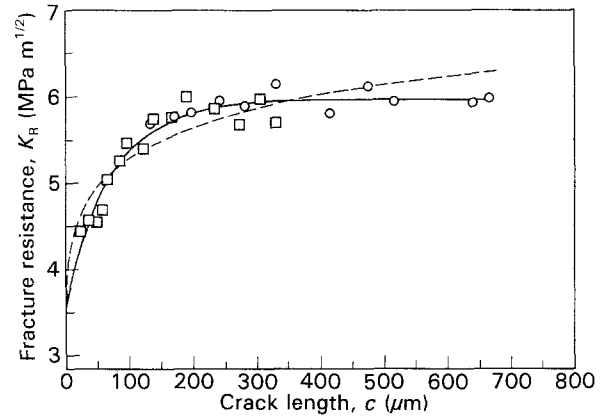


*Figure 5* Rising crack-growth-resistance (R-Curve) for SiC(whisker)-reinforced alumina: (⊡) initial crack length, $c_0$; (⊙) instability crack length, $c^*$; (—) exponential fit (crack-length data); and (- - -) power-law fit (crack-length data).

silicon nitride and the SiC(whisker)-reinforced alumina, respectively. Two interesting features common to the R-curves of both toughened ceramics are: (a) the overlap of the fracture toughnesses based on the two different sets of crack-length measurements, thus, defining the overall form of the R-curves; and (b) evidence of a plateau in the fracture toughnesses at large crack lengths. These two features, combined with the reasonable prediction of toughening ($\Delta K$) in SiC(whisker)-reinforced alumina based on theoretical models of whisker reinforcement [15], validated this method of R-curve measurement. In this study, the validity of the R-curves is further examined by predicting the indentation fracture strengths of the two ceramics. This is possible only through the use of analytical fits to the R-curves of the toughened ceramics.

## 2.3. Analytical functions for R-curves

As indicated in the introduction, the main objective of this study was to see if R-curves assessed by direct crack-length measurements can be used to predict the fracture strengths of indented ceramic specimens, and

TABLE I Elastic modulus, $E$, hardness, $H$, and crack-growth-resistance parameters, $K_0$, $K_\infty$, $\lambda$, $A$ and $n$, of silicon nitride and SiC(whisker)-alumina

| Property | Silicon nitride | SiC(whisker)-alumina |
|---|---|---|
| Young's modulus[a], $E$(GPa) | 310 | 380 |
| Hardness[b], $H$ (GPa) | 14.82 | 17.81 |
| R-curve parameters | | |
| $K_0$ (MPa m$^{1/2}$) | 6.66 | 3.57 |
| $K_\infty$ (MPa m$^{1/2}$) | 10.16 | 5.96 |
| $\lambda$ ($\mu$m) | 201.27 | 71.08 |
| Correlation coefficient, $r$ | 0.96 | 1.00 |
| R-curve parameters | | |
| $A$ (MPa m$^{1/2}$ m$^{-n}$) | 26.04 | 12.40 |
| $n$ | 0.127 | 0.093 |
| Correlation coefficient, $r$ | 0.95 | 0.94 |

[a] Reported by the material suppliers.
[b] Experimental values from a previous study [15].

then to examine the sensitivity of the relation between log fracture-strength and log indentation-load to the analytical functions chosen to fit the R-curves. The first function chosen was a simple power law of the form:

$$K_R(c) = Ac^n \quad (6)$$

where $A$ and $n$ are empirical parameters that describe the R-curve. Equation 6 was selected because it is commonly inferred from a linear plot of log strength versus log indentation-load [7–11]. The values of the parameters $A$ and $n$ determined by minimizing the total variance by iterative linear regression, and the respective correlation coefficients are listed in Table I. The corresponding fits of Equation 6 are shown by the dashed lines in Figs 4 and 5. The power law overestimates the fracture toughness at long crack lengths and does not provide for a plateau in the toughness.

Because of the plateau in the fracture toughness evident in both R-curves and since a lower-bound fracture toughness is physically realistic [23, 24], the following function was chosen to fit the fracture-toughness data:

$$K_R(c) = K_\infty - (K_\infty - K_0)\exp\left(-\frac{c}{\lambda}\right) \quad (7)$$

In Equation 7, $K_\infty$ and $K_0$ are plateau and lower-bound fracture toughnesses, respectively, and $\lambda$ is a crack-length normalizing parameter. The solid lines in Figs 4 and 5 represent best fits of Equation 7 to the measured R-curve data. The corresponding best-fit values of the parameters $K_\infty$, $K_0$ and $\lambda$, obtained by iterative linear regression and minimum total variance, and of the correlation coefficients are listed in Table I. It should be noted that Equation 7 gave better fits to the R-curves of both ceramics.

## 2.4. Prediction of indentation-load dependence of fracture strengths

The fracture instability and strength of a ceramic that exhibits rising crack-growth resistance are governed

by the following conditions [12, 13]:

$$K_a = K_R(c) \tag{8}$$

$$\frac{dK_a}{dc} > \frac{dK_R(c)}{dc} \tag{9}$$

In Equations 8 and 9, $K_a$ is the crack-driving force expressed in terms of the applied stress intensity. For a surface crack produced by Vickers indentation, $K_a$ is a function of the crack length, the applied far-field stress, $\sigma$, and the indentation load, $P$:

$$K_a(c, \sigma, P) = \delta\left(\frac{E}{H}\right)^{1/2} \frac{P}{c^{3/2}} + 2\Omega\sigma\left(\frac{c}{\pi}\right)^{1/2} \tag{10}$$

It should be noted that the right-hand side of Equations 2 and 10 are identical. However, there is an important difference in the application of the two equations. Equation 2 is employed to define crack-growth-resistance only when the applied stress intensity and the crack-growth resistance exactly balance and the stably growing crack is in quasistatic equilibrium. Equation 10, on the other hand, defines the applied stress intensity for any combination of crack length, applied far-field stress and indentation load. Equations 4 and 5 were used to define $\Omega$ of Equation 10 for strength predictions of silicon nitride and SiC(whisker)-reinforced alumina, respectively.

Together, Equations 8 and 9 imply that unstable fracture occurs at that particular combination of crack length and far-field stress for which the $K_a$ curve is tangential to the R-curve. Accordingly, for each indentation load, the crack length and far-field stress that satisfy Equations 8 and 9 were determined numerically. This procedure was applied to all indentation loads that were used in the experimental measurements of fracture strengths. Graphical confirmation of the numerically based predictions was obtained by plotting $K_a$ as a function of $c$, (that is, plotting $K_a(c)$) for various stress levels and inspecting for tangency. This is illustrated in Fig. 6 for silicon nitride where the solid line represents the $K_R(c)$ or the R-curve as expressed by the best-fit exponential function of Equation 7, and the dashed lines represent the crack-driving force or $K_a(c)$ curves for selected indentation loads. Each of the $K_a(c)$ curves shown in Fig. 6 depicts tangency and in turn the prediction for crack length and far-field stress that leads to specimen instability in flexure for a specific indentation load. The numerical values of the predicted fracture strengths, $\sigma_f$, for the corresponding load, $P$, are also listed in Fig. 6. A similar analysis was carried out using the power-law fit to the R-curves of both ceramics.

## 3. Results and discussion

Fig. 7 shows a plot of fracture stress versus indentation load for silicon nitride. The discrete points are the measurements in four-point bending. The solid line represents the prediction of strength based on the R-curve described by the exponential function of Equation 7. The dashed line represents a strength prediction based on the power law of Equation 6. It is evident from Fig. 7 that strength predictions based on both analytical functions are slightly greater than the experimental data. However, the exponential function gave the better prediction of these two functions. This result is not surprising in view of the overall better fit of the exponential function to the R-curve data in Fig. 4. The greater deviation of the power-law prediction to higher strengths is consistent with the deviation of the power-law fit to higher fracture toughnesses at long crack lengths (see Fig. 4). Secondly, the prediction based on the exponential function is quite linear on the log fracture-stress versus log indentation-load plot in the limited range of indentation loads used in the experiments.

The non-linear log fracture-stress versus log indentation-load relation predicted in Fig. 7 on the basis of the power-law R-curve is different from the linear prediction used in past studies [7–11]. The difference lies in the treatment of the stress-intensity coefficient, $\Omega$. In the present study, the variation of $\Omega$ with crack size and shape was taken into account using Equations 3 to 5 and incorporated into the numerical/graphical analysis. Past studies used a closed-form analytical relation between the fracture strength and the indentation load which was based on the power-law function for the R-curve and the assump-

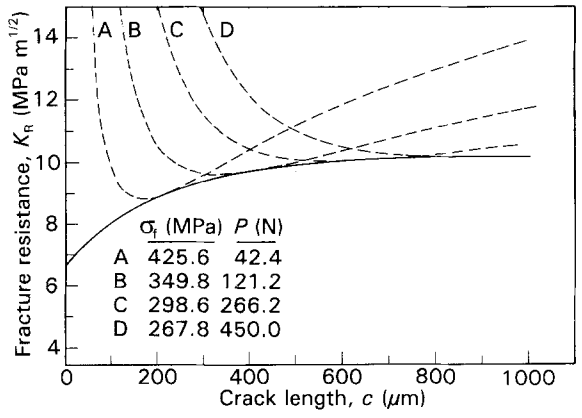


*Figure 6* A graphical construction demonstrating instability conditions for Vickers cracks in a toughened ceramic exhibiting rising crack-growth-resistance in silicon nitride: (—) R-curve (exponential fit), and (- - -) crack-driving force.

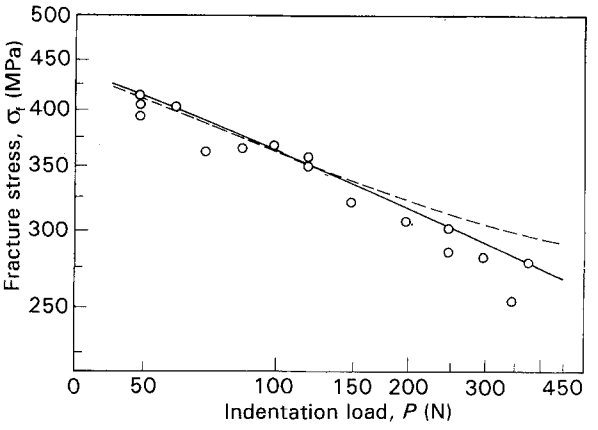


*Figure 7* Variations of the fracture strength with the indentation load for silicon nitride: (○) experimental data, (—) a prediction based on Equation 7, and (- - -) a prediction based on Equation 6.

tion that $\Omega$ is constant and independent of the crack size and shape. Under these conditions, the relationship between the fracture strength and the indentation load is given by the following equation [7]:

$$\sigma_f = \frac{(3 + 2n)\pi^{1/2}A}{8\bar{\Omega}}\left[\frac{(1 - 2n)A}{4\delta(E/H)^{1/2}P}\right]^{(1-2n)/(2n+3)} \quad (11)$$

In Equation 11, $\Omega$ is written as $\bar{\Omega}$ to emphasize that it is assumed constant. Thus, a plot of $\log \sigma_f$ versus $\log P$ should yield a straight line with a slope related to the power-law exponent, $n$. Equation 11 has been used as a basis of estimating $n$ and $A$, the parameters of the power-law R-curve, from $\log \sigma_f$ versus $\log P$ plots in several studies [7–11].

Fig. 8 shows experimental data and predictions of the fracture strength as a function of the indentation load for the SiC(whisker)-reinforced alumina. The trends in the fracture-strength predictions based on the two analytical R-curve functions relative to the experimental results are similar to those noted for silicon nitride.

The results shown in Figs 7 and 8 indicate that the fracture instability conditions of Equations 8 and 9 and the combined graphical/numerical procedure of Fig. 6 provide reasonable predictions of $\log \sigma_f$ versus $\log P$ for both ceramics. However, quantitatively, the strength predictions based on both analytical R-curve functions are slightly on the high side. A potential reason for this overestimation of the predicted fracture strengths is the overestimation of the fracture toughnesses or R-curves. In this regard, the residual-stress parameter, $\delta$, represents a potential source of error. The applied indentation force is related by $\delta$ to the residual crack-opening force of the plastic zone. Expressions for $\delta$ have been developed by Shetty *et al.* [18] for two limiting cases; one case treats the plastic zone associated with the indentation as a spring with zero compliance (rigid-wedge model), and the other treats it as a spring with infinite compliance (constant-force model). In the rigid-wedge model $\delta = 0.014$ and there is no stable crack extension; that is, $c^* = c_0$. On the other hand, in the constant-force model $\delta = 0.023$ and there is maximum stable crack growth; that is, $c^*/c_0 = 2.52$ for materials with flat crack-growth resistance. For materials with R-curve behaviour, the extent of stable crack growth is greater. The measured extent of stable crack growth, $c^*/c_0$, was $2.26 \pm 0.18$ for silicon nitride and $2.06 \pm 0.11$ for SiC(whisker)-reinforced alumina. These values of $c^*/c_0$ were approximately constant over the range of indentation loads employed for the two materials. The applicable values of $\delta$ for the two materials are, therefore, expected to be between 0.014 and 0.023, but are likely to be closer to 0.023. Therefore, the choice of the value 0.023 for $\delta$ might be one source of the overestimation of the fracture toughness. Since the compliance of the plastic zone relative to that of a surface crack increases with crack growth, $\delta$ is also expected to increase slightly with indentation load and crack growth [25].

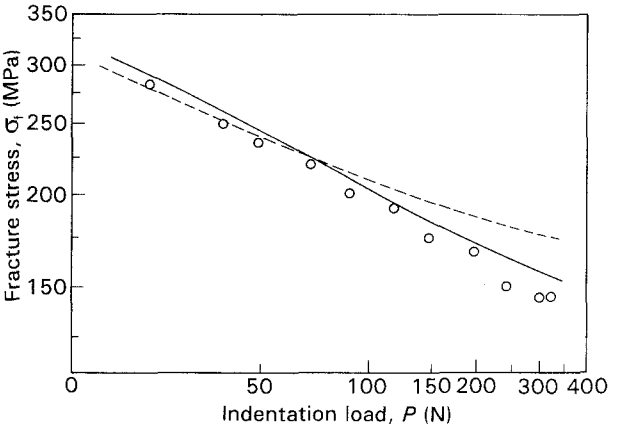


*Figure 8* Variations of the fracture strength with the indentation load for SiC(whisker)-reinforced alumina: (⊙) experimental data, (—) a prediction based on Equation 7, and (- - -) a prediction based on Equation 6.

The results of this study offer yet another perspective on the question of whether R-curve evaluations can be based on strength measurements alone.The apparent linearity of the log fracture-strength versus log indentation-load plots is usually cited as evidence in support of a power-law R-curve. But such a claim is not consistent with the results presented here. First, even if the R-curve can be described by a power-law, a precise strength analysis that takes into account crack size and shape effects on $\Omega$ predicts non-linear $\log \sigma_f$ versus $\log P$ plots (see Figs 7 and 8). Secondly, other candidate functions, such as the exponential function of Equation 7, predict an almost linear variation of $\log \sigma_f$ with $\log P$. It is, therefore, inappropriate to select an R-curve function based only on the indentation-load dependence of the fracture strength. Analytical R-curve functions should be selected to fit unbiased fracture toughness/crack length data based on physical considerations such as mechanistic models of toughening. Unfortunately, theoretical treatments of toughening, such as whisker reinforcement [24] or transformation-zone shielding [23], either do not explicitly predict R-curves or the predictions are in the form of numerical results. Nevertheless, assessment of R-curves based on direct crack-length measurements, as done in the present study, allows the use of the prediction of the indentation-load dependence of fracture strength to test the validity of the R-curves.

## 4. Conclusions

1. R-curves should be evaluated by direct measurements of crack lengths. Initial crack lengths upon indentation and instability crack lengths measured using multiple indents are convenient for such measurements. The advantages of the crack-length-based R-curve evaluation are that it is unbiased and it allows for a more precise calculation of the stress intensities of surface cracks.

2. The fracture strengths of Vickers-indented bend specimens can be accurately predicted from R-curves based on crack-length measurements. This prediction can be used as a means of validating the measured R-curves.

3. Linear plots of log fracture-strength versus log indentation-load with the magnitude of the gradient less than 1/3 are not adequate evidence in support of a power-law function for the R-curves. Widely differing analytical functions that can be fitted to R-curves result in similar and approximately linear log fracture-strength versus log indentation-load relations.

## Acknowledgements

This paper is based on research supported by the US Department of Energy under Contract No. DE-FG02-87ER45312 at the University of Utah. The authors are grateful to C. Griffin of Ceramatec, Inc. and D. Carruthers of Allied Signal Aerospace Co. for providing the SiC(whisker)-reinforced alumina and silicon-nitride ceramics employed in this study.

## References

1. A. G. EVANS, *J. Amer. Ceram. Soc.* **73** (1990) 187.
2. D. B. MARSHALL and M. V. SWAIN. *ibid.* **71** (1988) 399.
3. D. B. MARSHALL, *ibid.* **69** (1986) 173.
4. R. W. STEINBRECH and O. SCHMENKEL, *ibid.* **71** (1988) C271.
5. C. S. YU and D. K. SHETTY, *J. Mater. Sci.* **25** (1990) 2025.
6. R. F. COOK, B. R. LAWN and C. J. FAIRBANKS, *J. Amer. Ceram. Soc.* **68** (1985) 604.
7. R. F. KRAUSE Jr, *ibid.* **71** (1988) 338.
8. C. W. LI and J. YAMANIS, *Ceram. Engng. Sci. Proc.* **10** (1989) 632.
9. R. F. KRAUSE Jr, E. R. FULLER Jr and J. F. RHODES, *J. Amer. Ceram. Soc.* **73** (1990) 559.
10. J. HOMENY and W. L. VAUGHN, *ibid.* **73** (1990) 2060.
11. S. SRINIVASAN and R. O. SCATTERGOOD, *J. Mater. Res.* **5** (1990) 1490.
12. R. F. COOK and D. R. CLARKE, *Acta Metall.* **36** (1988) 555.
13. D. K. SHETTY and J. S. WANG, *J. Amer. Ceram. Soc.* **72** (1989) 1158.
14. R. M. ANDERSON and L. M. BRAUN, *ibid.* **73** (1990) 3059.
15. N. RAMACHANDRAN and D. K. SHETTY, *ibid.* **74** (1991) 2634.
16. R. F. COOK and B. R. LAWN, *ibid.* **66** (1983) C-200.
17. B. R. LAWN, A. G. EVANS and D. B. MARSHALL, *ibid.* **63** (1980) 574.
18. D. K. SHETTY, A. R. ROSENFIELD and W. H. DUCKWORTH, *ibid.* **68** (1985) C-65.
19. P. M. SCOTT and T. W. THORPE, *Fatigue Engng. Mater. Struct.* **4** (1981) 291.
20. M. KAWAHARA and M. KURIHARA, "Fracture 1977", Vol. 2, International Conference on Fracture, fourth series (ICF4), Waterpool, Canada (1977) p. 1361.
21. J. C. NEWMAN Jr, and I. S. RAJU, *Engng. Fract. Mech.* **15** (1981) 185.
22. ASTM Standard E. 740-80, "ASTM annual book of standards", Vol. 03.01 (American Society for Testing and Materials, Philadelphia, PA, 1984) pp. 740–51.
23. R. M. McMEEKING and A. G. EVANS, *J. Amer. Ceram. Soc.* **65** (1982) 242.
24. P. F. BECHER, C. H. HSUEH, P. ANGELINI, and T. N. TIEGS, *ibid.* **71** (1988) 1050.
25. D. K. SHETTY, A. V. VIRKAR, A. R. ROSENFIELD and W. H. DUCKWORTH, *ibid.* **67** (1984) C-201.

*Received 20 July 1992*
*and accepted 1 May 1993*